ACS OMEGA

http://pubs.acs.org/journal/acsodf

Article

Study on the Adsorption Properties of Oxalic Acid-Modified Cordierite Honeycomb Ceramics for Neutral Red Dyes

Shuhui Yang, Qingyan Cheng,* Liangyan Hu, Yunhan Gu, Yanji Wang, and Zhenfa Liu

Cite This: *ACS Omega* 2023, 8, 11457−11466

Read Online

ACCESS | Metrics & More | Article Recommendations

ABSTRACT: Removal of organic dyes from water by monolithic adsorbents is considered as an efficient and no-secondary pollution method. Herein, for the first time cordierite honeycomb ceramics (COR) treated with oxalic acid (CORA) were synthesized. This CORA exhibits outstanding removal efficiency toward the azo neutral red dyes (NR) from water. After optimizing the reaction conditions, the highest adsorption capacity of 7.35 mg·g^{-1} and a removal rate of 98.89% could be achieved within 300 min. Furthermore, investigation of the adsorption kinetics indicated this adsorption process could be described as a pseudo-second-order kinetic model with k_2 and q_e of 0.0114 g·mg^{-1}·min^{-1} and 6.94 mg·g^{-1}, respectively. According to the fitting calculation, the adsorption isotherm could also be described as the Freundlich isotherm model. The removal efficiency could be maintained above 50% after 4 cycles, negating the need for toxic organic solvent extraction, offering a method for bringing the technology one step closer to industrial application and giving CORA promising potential in practical water treatment.

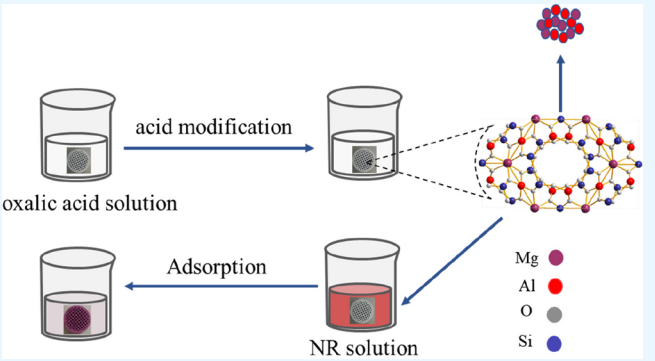

1. INTRODUCTION

A significant amount of waste is produced as a result of the population's rapid growth, human society's rapid development, and extensive agricultural practice.[1] Human life and health are in danger due to water pollution.[2−4] Since dyes are used in the printing and dyeing industries to color products, these industries have become the focus of wastewater treatment.[5−7] The dark organic dye wastewater pollutants will reduce sunlight's ability to pass through water and impact aquatic plants.[8,9] Additionally, toxic substances are highly concentrated and difficult to degrade,[10] and dyes may be mutagenic and carcinogenic to aquatic organisms, which could seriously harm human health[11,12] and cause serious environmental pollution.[13]

Wastewater discharged during cationic dye manufacturing and dyeing can cause allergic dermatitis, neurological diseases, rashes, cancer, and mutations.[14] The positively charged cationic dye molecule is soluble in water and creates colored cations in the solution. Wastewater from printing and dyeing processes frequently contains the cationic dye neutral red (NR). After entering the water, NR's high color development and low light transmittance seriously impede the body of water's ability to purify itself and result in extremely serious water pollution.[15] Consequently, it is crucial to effectively remove NR dyes from wastewater.

Different techniques have been used so far to treat wastewater.[16,17] Membrane filtration,[18] adsorption,[19,20] precipitation,[21] coagulation,[22] microbial degradation,[23] and photocatalytic and electrocatalytic degradation[24,25] are examples of traditional technologies. These techniques have some benefits, but they also have some drawbacks. For instance, membrane filtration offers low energy consumption, simple process control, and advanced wastewater treatment for printing and dyeing. But, it has significant fouling and incomplete degradation by biological and photodegradation methods.[26,27] The most competitive technology among them is adsorption technology. It can accomplish both the recycling of organic dyes and the purification of wastewater. Additionally, low costs, straightforward operations, no toxic materials, and high process efficiency also meet the requirements of green chemistry.[28] To clean up wastewater, some common adsorbents have been used, including various activated carbon adsorbents made of carbon and metal and non-metal oxide adsorbents.[29,30] The adsorption process still has some issues, even though these materials can effectively adsorb dyes in the solution.[31,32] For instance, most adsorbents have low stability and adsorption capacity, and pH has a significant impact on adsorption.[33]

Received: January 15, 2023
Accepted: March 8, 2023
Published: March 20, 2023

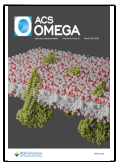

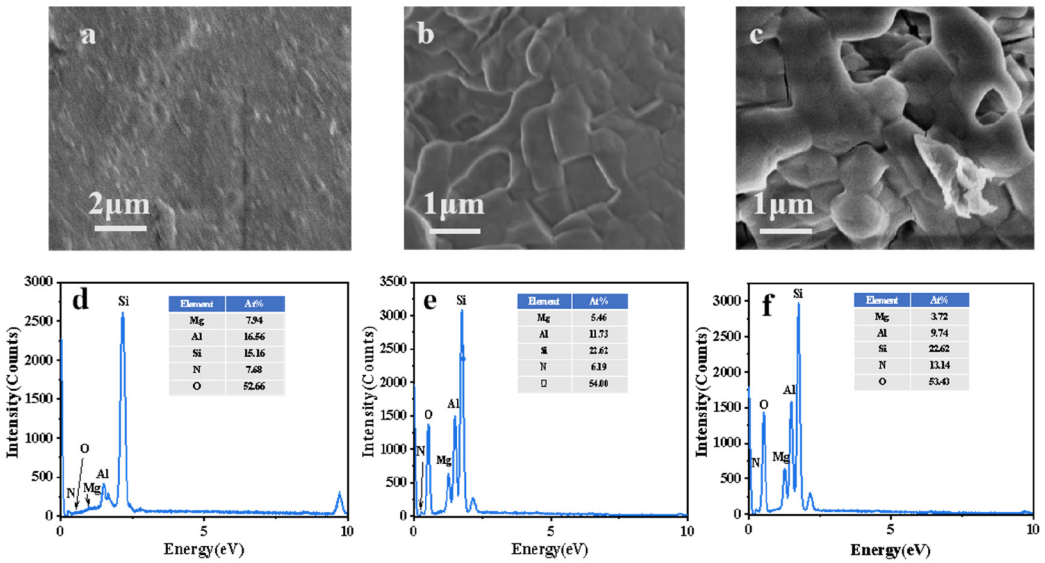

Figure 1. SEM photographs of the samples: (a) COR, (b) CORA, and (c) CORA-NR. EDX spectroscopy of COR (d), CORA (e), and CORA-NR (f).

Additionally, these adsorbents are challenging to recover and are not conducive to reuse or recycle. The monolithic adsorbent has proven to be a practical and affordable way to remove a variety of pollutants in some research.[34−37] For instance, porous ceramic membranes (PCMs), which are monolithic catalysts, have many applications in mass and heat transfer, and PCMs offered more active sites for the reactant gases during the catalytic reaction process than the powder catalysts did.[38] In one study, the monolithic catalysts of diatomite-modified wood ceramics have been widely used for the adsorption of pollutants due to their large specific surface area, strong adsorption capacity, and lower cost.[39]

Compared to conventional pellets or powder catalysts, which have the drawbacks of a low recycling rate and difficult recovery in an aqueous solution, cordierite honeycomb ceramics (COR), which have a high specific surface area,[40] high permeability, high adsorption capacity, relatively high mechanical strength,[41,42] inherent high porosity,[43] and low cost, were chosen as adsorbents.[44,45] In this paper, oxalic acid was used to simply modify cordierite honeycomb ceramics (CORA), and the effectiveness of NR dyes in solution adsorption was assessed. In the study of pollutant removal from NR-contaminated wastewater, the materials' rate of utilization was not only improved, but the results were also satisfactory.

2. MATERIALS AND METHODS

2.1. Materials. All of the agents are readily available on the market, and no additional purifications were done before reactions. Cordierite honeycomb ceramics (16 mm × 120 mm) were purchased from New Material Co., Ltd., Pingxiang City, Jiangxi Province. Oxalic acid ($H_2C_2O_4$) was purchased from Tianjin Chemical Reagent Factory. Neutral red ($C_{15}H_{17}N_4Cl$) was purchased from Tianjin Ruijinte Chemical Co., Ltd. Sodium hydroxide (NaOH) and hydrochloric acid (HCl) were purchased from Tianjin Komio Chemical Reagent Co., Ltd. Ethanol(C_2H_5OH) was purchased from Tianjin Fengchuan Chemical Reagent Technology Co., Ltd. Analytical-grade pure chemicals and reagents were used in this experiment without the use of any additional purification techniques.

2.2. Preparation of CORA. Commercially available honeycomb cordierite was used to make the cuts with $D \times L$ = 16 mm × 10 mm. After being exposed to an oxalic acid solution for 2 h at 358 K, the material was washed with distilled water until the washing solution was neutral, dried for 2 h at 353 K, and then calcined for 4 h at 773 K to remove the attached oxalic acid.

2.3. Characterization. Fourier transform infrared (FTIR, Nicolet iS50, USA) was used to analyze the functional groups on the surface of the adsorbents. An X-ray diffractometer (XRD, X'Pert PRO, Holland) was used to determine the crystal structure of CORA. Brunauer−Emmett−Teller (BET, ASAP2420-4MP, USA) surface area analysis was used to evaluated the CORA specific surface area and pore structure. X-ray photoelectron spectroscopy (XPS, ESCALAB 250Xi, England) was used to examine the chemical compositions and element states of CORA before and after NR adsorption. Zetasizer Nano (Zeta, ZS90) was used to determine the charge state on the surface. Scanning electron microscopy (SEM, SU8020) images and energy-dispersive X-ray (EDX) spectroscopy of CORA were used to compare before and after adsorbing NR dye.

2.4. Adsorption Experiments. The adsorption experiments of CORA were carried out by the batch method. Influencing factor experiments, such as oxalic acid concentration (0−40%), solution pH (3−7), NaCl concentration (0−100 mmol·L^{-1}), adsorbent dosage (10−30 mg·mL^{-1}), initial dye concentration range (20−100 mg·L^{-1}), contact time interval, and temperature (298−318 K) on adsorption of the dye were studied. The absorbance of NR was measured using an ultraviolet spectrophotometer (Shanghai Yidian Co., UV-L5) according to the absorbance at 530 nm. The standard curve of NR concentration absorption was drawn by measuring the absorbance. To evaluate the adsorption kinetics at a specific time interval, at time t, the adsorption capacity of the NR dye (q_t (mg·g^{-1})) and the percentage of the NR removal rate are expressed by the following equations

https://doi.org/10.1021/acsomega.3c00305
ACS Omega 2023, 8, 11457−11466

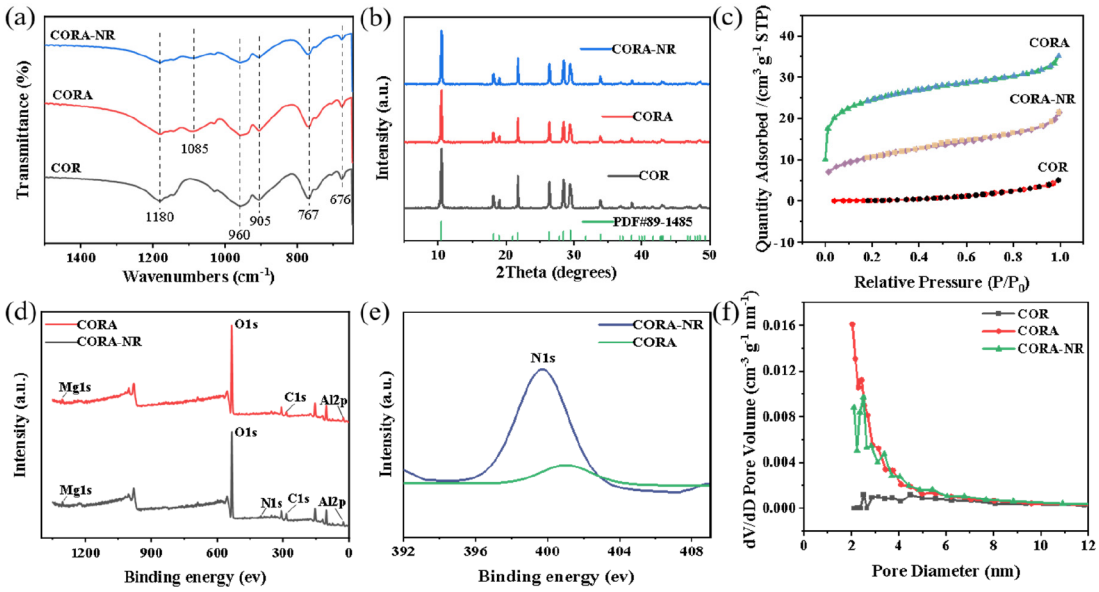

Figure 2. (a) FTIR spectra, (b) XRD patterns, (c) N_2 adsorption−desorption isotherms, (d) survey XPS spectra, (e) high-resolution N 1s XPS spectra of CORA before and after adsorption of NR, and (f) pore size distribution curves of COR, CORA, and CORA-NR.

$$q_t = \frac{(C_0 - C_t) \times V}{m} \quad (1)$$

$$R\ (\%) = \frac{C_0 - C_t}{C_0} \times 100\% \quad (2)$$

where C_0 is the initial NR concentration ($mg{\cdot}L^{-1}$), C_t is the NR concentration at any time t or equilibrium ($mg{\cdot}L^{-1}$), R (%) is the removal rate of the dye, V is the NR solution volume (L), and m is the mass of CORA (g).

2.5. Desorption and Regeneration Experiments. The recyclability of CORA was evaluated after treating the used adsorbent with deionized water. To desorb NR-loaded CORA, different desorbing solutions were used (t = 300 min, adsorbent dose = 15 $mg{\cdot}mL^{-1}$, C_0 = 20 $mg{\cdot}L^{-1}$, T = 298 K, pH = 7). After desorption, the used CORA was reused to adsorb NR, and the adsorption conditions were the same as those for the first adsorption process. The desorption efficiency (D) and regeneration efficiency (η) were calculated using the following equations

$$D = \frac{m}{m_c} \times 100 \quad (3)$$

$$\eta = \frac{q_n}{q_e} \times 100 \quad (4)$$

where D is the adsorption efficiency of CORA (%), m is the mass of NR (g), which was desorbed from the adsorbent, and m_c is the remaining NR mass on CORA before desorption (g). η is the regeneration efficiency of CORA (%), and q_n and q_e are the adsorption quantity of the regenerative CORA for recycle times and the primitive CORA in the same experimental conditions, respectively.

3. RESULTS AND DISCUSSION

3.1. Characterization of Materials. The prepared CORA was characterized by FTIR spectroscopy, XRD, N_2 adsorption−desorption experiment, XPS, SEM, and EDX spectroscopy.

3.1.1. SEM and EDX Analysis. The morphological characterization of COR, CORA, and CORA-NR was observed by SEM, Figure 1. The elemental compositions and contents of COR, CORA, and CORA-NR were qualitatively and quantitatively analyzed by EDX spectroscopy. The morphology of CORA had no obvious difference from CORA-NR. It was clearly observed that the surface of CORA has many pits because acid corrosion dissolves magnesium ions and aluminum ions, resulting in micropores and mesopores and making the surface more rough. This structure is more conducive to the adsorption of NR. EDX spectroscopy on the variation of the Mg and Al contents in COR and CORA prove this in Figure 1d and 1e, respectively. As shown in Figure 1e and 1f, the elements Mg, Al, Si, N, and O are detected. The N element increased after the adsorption, which meant CORA had adsorbed NR successfully; the same XPS test results can also prove this.

3.1.2. FTIR Analysis. FTIR spectroscopy is a vital tool to characterize both the covalent and the noncovalent functional groups of a substance. The FTIR spectra of COR, CORA, and CORA following adsorption of NR (CORA-NR) are shown in Figure 2a. The absorption peak near 1180 cm^{-1} was the Si−O absorption peak of COR, and the peak at around 1085 cm^{-1} was the SiO_4 tetrahedral antisymmetric stretching vibration absorption peak. The Si−OH end group's symmetric stretching vibration absorption peak was at 960 cm^{-1}, the SiO_4 tetrahedron's symmetric stretching vibration absorption peak was at 767 cm^{-1}, and the bending vibration peaks of Si−O−Si and Si−O−H in CORA were at 905 and 676 cm^{-1}, respectively.[46] Compared with COR, CORA showed a peak at around 1085 cm^{-1}; this may be due to the removal of Al^{3+} and Mg^{2+} from the cordierite structure by oxalic acid treatment, destroying the silicate structure of cordierite.[40] The following BET and XPS test results also confirm these results.

3.1.3. XRD Analysis. The XRD patterns of COR, CORA, and CORA-NR are displayed in Figure 2b. Compared with COR, the characteristic peaks of CORA were slightly weaker after acid treatment. It can be seen that the XRD patterns of COR, CORA, and CORA-NR are essentially unchanged, and

https://doi.org/10.1021/acsomega.3c00305
ACS Omega 2023, 8, 11457−11466

Table 1. Comparison of the Main Elemental Contents before and after Oxalic Acid Modification

	COR				CORA			
	Al	Mg	Si	O	Al	Mg	Si	O
content (%)	18.58	8.1	23.3	48.58	2.83	1.31	25.67	65.66

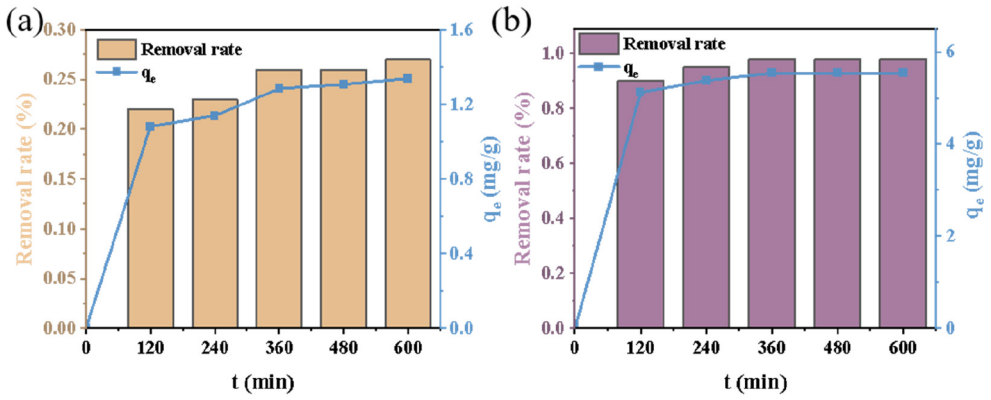

Figure 3. (a) The adsorption capacity and removal rate of COR. (b) The adsorption capacity and removal rate of CORA. Adsorption conditions: C_0 = 20 mg/L; amount of CORA = 15 mg/mL; T = 298 K; t = 300 min; pH = 7.

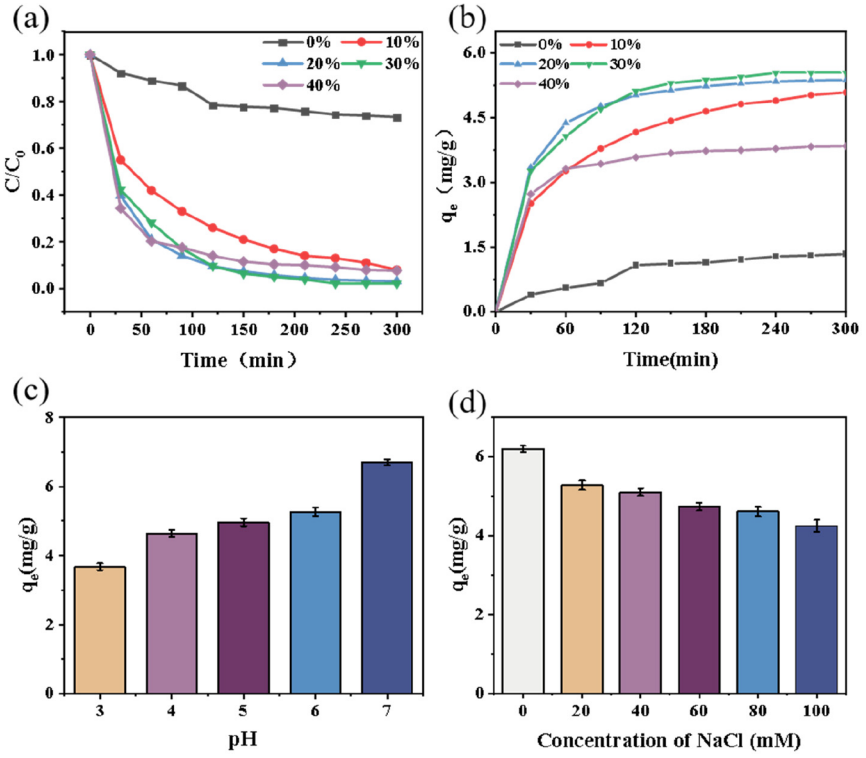

Figure 4. Removal rate (a) and adsorption capacity (b) of NR by COR modified with different concentrations of oxalic acid. (c) Effect of pH on adsorbing NR. (d) Influence of NaCl on the adsorption capacity of CORA. Adsorption conditions: C_0 = 20 mg/L; amount of CORA = 15 mg/mL; T = 298 K; t = 300 min.

the intensity and position of the diffraction peaks were essentially the same. This showed that the main crystallite structure was stable even after oxalic acid modification.

3.1.4. BET Analysis. To evaluate the porosity of the obtained adsorbent, the N_2 adsorption and desorption isotherms of COR, CORA, and CORA-NR adsorbents were obtained and are displayed in Figure 2c, and the pore size distributions are presented in Figure 2f. As shown in Figure 2c, CORA showed a type I isotherm that was specific to microporous materials. CORA had obvious microporous (<1.8 nm) and mesoporous (3.0−4.0 nm) structures, making its total pore volume (0.028 $cm^3 \cdot g^{-1}$) and specific surface area (80 $m^2 \cdot g^{-1}$) higher than those of COR (0.010 $cm^3 \cdot g^{-1}$, 0.94 $m^2 \cdot g^{-1}$). The BET test showed that oxalic acid modification produced micropores and mesopores and increased the specific surface area because the treatment of cordierite with oxalic acid is a chemical corrosion process. Micropores can be produced by directly removing metal ions from the surface of cordierite, but to produce

https://doi.org/10.1021/acsomega.3c00305
ACS Omega 2023, 8, 11457−11466

mesopores, some structural rearrangement seems necessary. This process may involve the destruction of the cordierite silicate structure under harsh oxalic acid treatment conditions. The XPS data also confirm that more than 80% of the Mg^{2+} and Al^{3+} are removed from the cordierite lattice.

3.1.5. XPS Analysis. In determining the ratio of each oxidation state of metals in the materials, XPS was extremely useful. The XPS results in Figure 2d indicated the presence of Mg, O, Al, and N elements in CORA and CORA-NR. Meanwhile, compared the XPS results of elements in Figure 2e, the N element appeared after the adsorption, which meant CORA had adsorbed NR successfully. Compared to the main element contents between COR and CORA (Table 1), as shown in the FTIR results, BET results, and the related literature,[40] it can be concluded that Al^{3+} and Mg^{2+} were removed from the cordierite structure by oxalic acid treatment. The silicate structure of the active solid was destroyed, resulting in the formation of a highly specific surface area of the active solid, which subsequently facilitates the adsorption of NR.

3.2. Adsorption Study. The various adsorption capacities of NR dye are depicted in Figure 3. Furthermore, under the conditions of an NR concentration of 20 $mg{\cdot}L^{-1}$, a temperature of 298 K, a pH of 7, and an adsorbent concentration of 15 $mg{\cdot}mL^{-1}$ for 300 min, the adsorption capacity of COR was 1.34 $mg{\cdot}g^{-1}$ and the removal rate was only 22.31%. Under the same conditions, the adsorption of NR dye on CORA was obviously enhanced. The adsorption capacity increased by 75.85% to 5.54 $mg{\cdot}g^{-1}$, and the removal rate was 98.89%, which was 76.58% higher than that of COR.

3.2.1. Effect of Oxalic Acid Concentration on Adsorption. Figure 4a and 4b shows that compared to COR, the adsorption capacity and removal rate of NR by COR modified with various concentrations of oxalic acid were higher. From the previous analysis of the specific surface area and pore volume, oxalic acid modification may affect the pore structure and specific surface area of CORA, which in turn affect the adsorption performance of CORA. As can be seen from Figure 4a and 4b, the effect of 10% oxalic acid modification was the least satisfactory. Internal micropores and mesopores also experience more corrosion of COR as oxalic acid concentrations rise.[40,47,48] However, the adsorption capacity and efficiency of CORA modified with 40% oxalic acid are lower than those of CORA modified with 20% and 30% oxalic acid. There are not many differences between COR modified by 20% and 30% oxalic acid in terms of adsorption effectiveness and capacity. Thus, 20% oxalic acid modification can essentially remove surface impurities, has the most suitable microporous and mesoporous structure, and will not result in a significant amount of raw material waste. In conclusion, a concentration of 20% oxalic acid modification is ideal.

3.2.2. Effect of pH on Adsorption. As is widely known, the system's pH level was a crucial factor in the adsorption process. The initial pH level will have an impact on the surface charge of CORA and the degree of protonation of NR. It can affect the morphology of NR in the aqueous phase and the surface charge of the adsorbent. Because the solubility of NR decreases in alkaline conditions, the pH range was between 3 and 7. Figure 4d displays the adsorption outcomes at various solution pH levels. The diagram makes it clear that as the pH value rises, the negative charge on the surface of CORA increases, making it easier to adsorb positively charged NR. As a result, the adsorption rate of CORA on NR rises and reaches saturation at pH = 7, indicating that pH = 7 was the most adsorption-friendly value. Since the pH of the untreated NR solution was around 7, there was no need to adjust it.

3.2.3. Effect of NaCl Concentration on Adsorption. The wastewater containing dye had a higher salt concentration, and the NaCl effect was of some importance in dye adsorption onto adsorbents. The effect of NaCl concentration on NR adsorption by CORA is shown in Figure 4e. It is seen that the increase in the NaCl concentration resulted in a decrease in the NR adsorption quantity, which could be attributed to a competitive effect between NR ions and sodium ions from the salt for the sites available for the adsorption process.[49] In addition, even at 100 $mmol{\cdot}L^{-1}$ NaCl, about 292 times the dye concentration, there was only a little decrease in the adsorption capacity. As a result, the high concentration of NaCl did not affect the selectivity of CORA adsorbent.

In summary, as the pH value rises, the negative charge on the surface of CORA increases, making it easier to adsorb positively charged NR, and the increase in the NaCl concentration resulted in a decrease in the NR adsorption quantity, which could be attributed to a competitive effect between NR ions and sodium ions from the salt for the sites available for the adsorption process. These results about the effect of pH and NaCl concentration imply that the main mechanism between CORA and NR was electrostatic attraction.

3.2.4. Effect of Dye Concentrations on Adsorption Isotherms. Adsorption isotherms were used to measure the relationship between adsorbents and adsorbates. Langmuir, Temkin, and Freundlich's models were used for the fitting analysis of experimental data.

The Langmuir isotherm model was typically used when the guest was evenly distributed over the adsorbents in monolayer coverage,[50] which is expressed as

$$q_e = \frac{K_L q_m C_e}{1 + K_L C_e} \tag{5}$$

where q_e is the maximum adsorption capacity ($mg{\cdot}g^{-1}$), q_m is the equilibrium adsorption capacity of NR on CORA ($mg{\cdot}g^{-1}$), K_L is a constant associated with the affinity of the binding sites and energy of adsorption ($L{\cdot}mg^{-1}$), and C_e is the equilibrium concentration of NR in the suspension ($mg{\cdot}L^{-1}$).

The Freundlich isotherm model[51] predicted nonuniform adsorption on heterogeneous adsorbents and was expressed as the following equation

$$q_e = K_F C_e^{1/n} \tag{6}$$

where K_F is the Freundlich isotherm constant and $1/n$ is a constant that relates to the adsorption intensity and capacity. The magnitude of the component n indicated favorability.

The Temkin isotherm model is expressed as the equation

$$q_e = A + B\ln C_e \tag{7}$$

where A and B are the Temkin isotherm constants.

According to the data calculated from the nonlinear fitting (Table 2 and Figure 5a) and the calculated coefficients (R^2), the Freundlich isothermal model could be considered the most suitable model to describe this adsorption behavior with a reliable correlation coefficient compared with that of the Langmuir model and the Temkin model. The parameters K_L (<1) and n (<1) indicate a homogeneous, monolayer, and favorable adsorption process. The range of n values from 1 to

https://doi.org/10.1021/acsomega.3c00305
ACS Omega 2023, 8, 11457−11466

Table 2. Adsorption Isotherm Parameters Calculated in Different Isothermal Models

Langmuir		
q_{max} (mg·g^{-1})	K_L (L·mg^{-1})	R^2
44.3790	0.07774	0.9697
Freundlich		
$1/n$	K_F (mg^{1-n}·L^{1-n}·g^{-1})	R^2
0.6099	4.3740	0.9840
Temkin		
A	B	R^2
3.4543	7.4407	0.9485

10 indicates advantageous adsorption. Table 2 displays the values of the Freundlich constants and the R^2 correlation coefficient. The value of $1/n$ was calculated to be between 0.1 and 1, indicating that the process of CORA adsorbing NR is more likely to occur and that CORA has some prospects for practical application.

3.2.5. Adsorption Kinetic Study. Adsorption kinetics research is desirable because it reveals details about the process' mechanism, which are crucial for raising the process' effectiveness. The experimental data were subjected to the application of several kinetic models, including pseudo-first-order, pseudo-second-order, and Elovich models. The effects of contact time and initial NR concentration on the adsorption of NR by CORA are shown in Figure 3. The amount of NR adsorbed onto CORA increased as time passed. Most of the NR molecules' adsorption took place in the initial 30 min of the experiment, and the adsorption rate was fast. The rate of adsorption slows over time. The pseudo-first-order kinetic model, pseudo-second-order model, and Elovich model are described with the following equations

$$\log(q_e - q_t) = \log q_e - \frac{K_1 t}{2.303} \tag{8}$$

$$\frac{t}{q_t} = \frac{1}{K_2 q_e^2} + \frac{t}{qe} \tag{9}$$

$$q_t = \frac{1}{\beta}\ln(\alpha\beta) + \frac{1}{\beta}\ln t \tag{10}$$

where q_e (mg·g^{-1}) is the equilibrium adsorption capacity, q_t (mg·g^{-1}) is the adsorption capacity measured at a contact time of t, K_1 (L·min^{-1}) and K_2 (g·mg^{-1}·min^{-1}) are the rate constants from the pseudo-first-order and pseudo-second-order kinetic models, respectively, α (mg·g^{-1}·min^{-1}) is the initial adsorption rate constant, and the parameter β (g·mg^{-1}) is the amount of surface covering and chemisorption activation energy.

According to Figure 5b–d and Table 3, the pseudo-second-order equation could best predict the dynamic adsorption of NR on CORA. The equilibrium adsorption capacity obtained from the pseudo-second-order model was closer to the experimental value than the equilibrium adsorption capacity obtained from the pseudo-first-order model. As a result, the pseudo-second-order models were used in the study to explain the NR adsorption behaviors. According to the results, NR was mainly absorbed on the surface of CORA, and the chemisorption transversion played a dominant role in the process. The electrostatic interaction and ion exchange reaction are the main driving forces for the adsorption process.

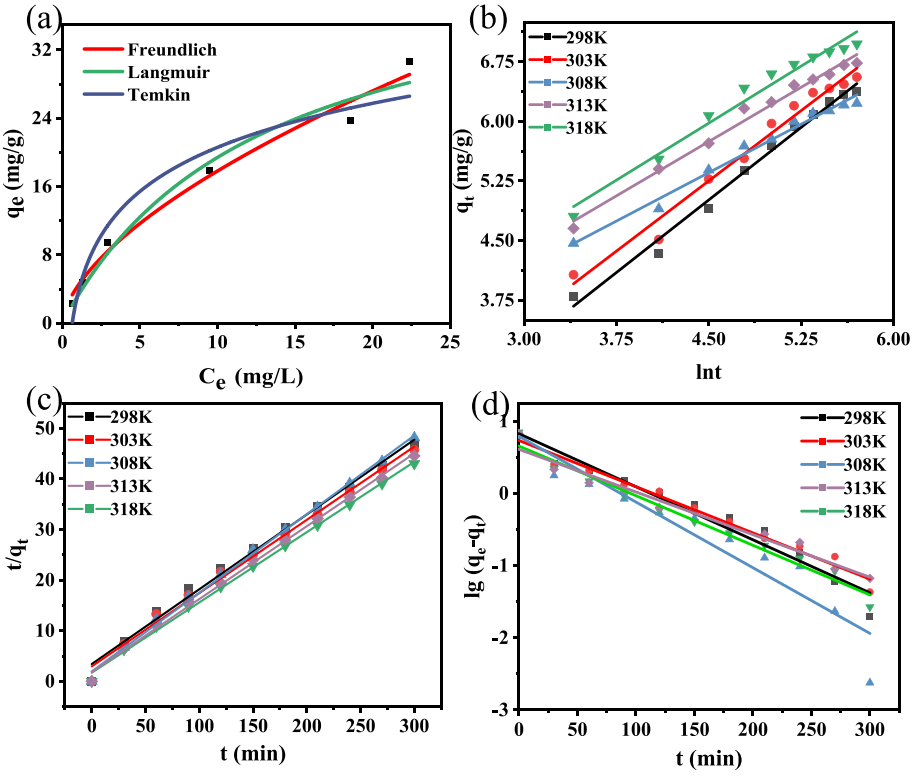

Figure 5. Adsorption data of NR on CORA: (a) nonlinear fitting of Langmuir, Temkin, and Freundlich isotherms models, (b) linear fitting of the Elovich kinetic model, (c) linear fitting of the pseudo-second-order kinetic model, and (d) linear fitting of the pseudo-first-order kinetic model.

https://doi.org/10.1021/acsomega.3c00305
ACS Omega 2023, 8, 11457−11466

Table 3. Kinetic Study of NR Adsorption on CORA at 298−318 K[a]

	pseudo-first-order kinetic model			pseudo-second-order kinetic model			Elovich		
T (K)	K_1 (min^{-1})	q_e (mg·g^{-1})	R^2	K_2 (g·mg^{-1}·min^{-1})	q_e (mg·g^{-1})	R^2	α (mg·g^{-1} min^{-1})	β (g·mg^{-1})	R^2
298	0.0169	6.71	0.9538	0.0063	6.76	0.9909	0.831	0.822	0.9890
303	0.0147	5.40	0.9793	0.0071	6.91	0.9927	1.130	0.849	0.9786
308	0.0210	6.16	0.9058	0.0115	6.43	0.9973	6.595	1.232	0.9844
313	0.0158	4.52	0.9750	0.0112	7.20	0.9977	5.525	1.046	0.9743
318	0.0136	4.07	0.9695	0.0114	6.94	0.9972	5.576	1.099	0.9861

[a]Adsorption conditions: C_0 = 20 mg/L; amount of CORA = 15 mg/mL; t = 300 min; pH = 7.

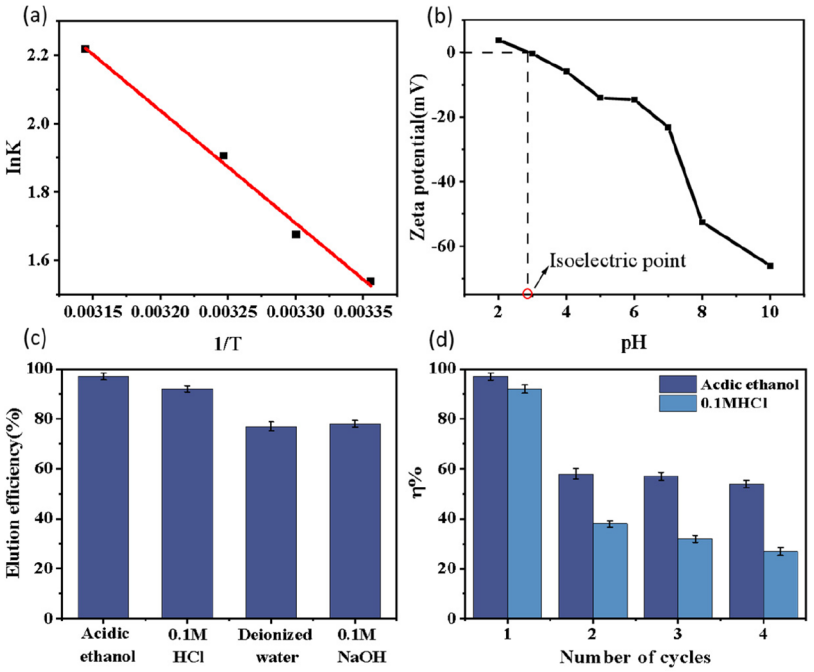

Figure 6. (a) Linear plot of ln K vs $1/T$ for the adsorption of NR by CORA. (b) The zeta potential of CORA. (c) The elution efficiency by different solutions. (d) The regeneration rate of four cycles using different solutions. Adsorption conditions: C_0 = 20 mg/L; amount of CORA = 15 mg/mL; T = 298 K; t = 300 min; pH = 7.

3.2.6. Thermodynamic Parameters. Thermodynamic studies could well describe the adsorption of NR on CORA. Thermodynamic parameters like the Gibbs free energy (ΔG), standard enthalpy change (ΔH), and standard entropy change (ΔS) were obtained by also looking into the thermodynamics of adsorption. Using the Van't Hoff equation, the parameters could be determined

$$\ln K = \frac{-\Delta H}{RT} + \frac{\Delta S}{R} \tag{11}$$

$$\Delta G = -RT \ln K \tag{12}$$

where K is the calculated adsorption equilibrium constant from q_e/c_e and ΔH and ΔS are obtained from the straight line plots of ln K against $1/T$ (Figure 6a).[52] Table 4 displays the computed parameters.

The reaction rate was physically measured by the activation energy (E_a), whose value could be used to determine the nature of the adsorption process. The Arrhenius formula was used to get the activation energy of the adsorption process, and the resulting linear equation was

$$\ln K_2 = \ln K_0 - \frac{E_a}{RT} \tag{13}$$

Table 4. Thermodynamic Parameters of CORA in the Adsorption of NR

T (K)	ΔG (kJ mol^{-1})	ΔH (kJ mol^{-1})	ΔS (J mol^{-1})	R^2
298	−3.813	27.38	104.5760	0.9937
303	−4.222			
308	−4.881			
313	−5.637			
318	−5.864			

where E_a (kJ·mol^{-1}) is the apparent activation energy of the adsorption reaction, K_0 (g·mg^{-1}·min^{-1}) is the temperature-independent factor, R (8.314 J mol^{-1} K^{-1}) is the gas constant, and T (K) is the adsorption absolute temperature. Plotting ln K_2 against $1/T$ resulted in a straight line with a slope of $-E_a/R$.

The positive ΔH value indicates that the adsorption of NR on CORA is an endothermic process. Meanwhile, the negative ΔG value indicates that adsorption occurred spontaneously at various temperatures, and adsorption was more likely to occur at higher temperatures as the adsorption capacity increased with temperature and the ΔG value decreased. The increment of ΔG (absolute value) at the increased temperature suggested that elevating the operation temperature could enhance the adsorption of NR onto activated CORA. Therefore, using activated CORA as an adsorbent for removing NR in water is

https://doi.org/10.1021/acsomega.3c00305
ACS Omega 2023, 8, 11457−11466

applicable. The value of E_a < 40 kJ·mol^{-1} is the result of the physical adsorption process. The energy of activation was calculated to be 23.79 kJ·mol^{-1} from the Arrhenius equation, confirming the occurrence of physical activity in the adsorption process.

3.2.7. Regeneration and Reuse. To verify the stability and reusability of CORA, the desorption and regeneration performance of different solvents on CORA were tested, and the reagents with better desorption and regeneration performance were used for further multiple recycling studies. H_2O, 0.1 mol·L^{-1} HCl, 0.1 mol·L^{-1} NaOH, and acidic ethanol were selected as the solvents for CORA study on the desorption regeneration performance. The experimental results are shown in Figure 6c and 6d. The desorption rate was the highest with an acidic ethanol solution as the desorption agent. First, the desorption was mainly due to the competitive adsorption between H^+ in acidic ethanol and cationic dye−neutral red molecules. Second, ethanol molecules can provide a certain polarization force to promote the desorption of dye.

After four cycles of adsorption and desorption experiments, the desorption rate of acidic ethanol remained above 50%, indicating that CORA still had high stability. This may be due to the chemical desorption process not being complete, resulting in some dye molecules still occupying the adsorption site of CORA. At the same time, the XRD pattern of CORA after adsorption did not change significantly, which proved that the CORA structure was not destroyed and was relatively stable. CORA was stable during the neutral red recovery process, and that recovery required neither organic solvents nor high concentrations of acids or bases. Therefore, this had great convenience for the practical application of targeted recovery of cationic dyes from printing and dyeing wastewater.[53−56]

3.2.8. Adsorption Mechanism. The zeta potential of CORA decreased with increasing pH value, and the negative charge increased gradually. The results show that the electrostatic adsorption ability of CORA for cationic dyes gradually increased, which is consistent with the changing trend of NR adsorption capacities under different pH conditions. The isothermal fitting results show that the adsorption process was a monolayer adsorption process on a heterogeneous surface. The kinetic and thermodynamic analysis results show that NR's chemical adsorption and physical adsorption on CORA occurred simultaneously. The effects of pH value and coexisting ions on the adsorption capacity show that ion exchange was also one of the adsorption mechanisms. It is also noted that the specific surface area of CORA was larger than that of COR, which could enhance the contact area between CORA and NR. In summary, the dye adsorption on CORA was a complex process, which may include multiple synergistic contributions, such as physical adsorption, electrostatic interaction, and ion exchange reaction.

4. CONCLUSION

In this work, based on the idea of green synthesis, CORA was successfully modified by different concentrations of oxalic acid for the first time. Then, the prepared CORA was used as an efficient porous adsorbent to remove organic dye NR from water. When the concentration of oxalic acid was 20%, CORA had a high specific surface area and abundant microporous and mesoporous pore structures. When the pH was equal to 7, the adsorption capacity was the highest. The addition of NaCl reduced the adsorption capacity significantly. The kinetic process study showed that the adsorption of dyes on the surface of CORA conformed to the pseudo-second-order kinetic model, indicating that there was a possibility of chemical adsorption between NR and CORA. The adsorption isotherm conforms to the Freundlich model. Thermodynamic analysis showed that the system is a spontaneous, endothermic, and physical process in nature. Finally, the reusability of CORA was tested. After four cycles, the maximum desorption rate of CORA can still be maintained at more than 50%. Therefore, CORA has ideal removal efficiency and good reusability, which provides an idea for the rapid separation of adsorbents from solution. It is a promising monolithic water treatment adsorbent.

AUTHOR INFORMATION

Corresponding Author

Qingyan Cheng − *School of Chemical Engineering and Technology, Hebei University of Technology, Tianjin 300401, China; Tianjin Key Laboratory of Chemical Process Safety, Tianjin 300401, China*; Email: chengqingyan@hebut.edu.cn

Authors

Shuhui Yang − *School of Chemical Engineering and Technology, Hebei University of Technology, Tianjin 300401, China*; orcid.org/0000-0002-3795-8621

Liangyan Hu − *School of Chemical Engineering and Technology, Hebei University of Technology, Tianjin 300401, China*

Yunhan Gu − *School of Chemical Engineering and Technology, Hebei University of Technology, Tianjin 300401, China*

Yanji Wang − *School of Chemical Engineering and Technology, Hebei University of Technology, Tianjin 300401, China; Tianjin Key Laboratory of Chemical Process Safety, Tianjin 300401, China*

Zhenfa Liu − *Institute of Energy Sources, Hebei Academy of Science, Shijiazhuang, Hebei Province 050081, China*; orcid.org/0000-0002-1243-4725

Complete contact information is available at: https://pubs.acs.org/10.1021/acsomega.3c00305

Notes

The authors declare no competing financial interest.

ACKNOWLEDGMENTS

This work was supported by the National Natural Science Foundation of China (U20A20152).

REFERENCES

(1) Jain, K.; Patel, A. S.; Pardhi, V. P.; Flora, S. J. S. Nanotechnology in Wastewater Management: A New Paradigm Towards Wastewater Treatment. *Molecules* **2021**, *26*, 1797.

(2) Zhao, Y.; Yang, H.; Sun, J.; Zhang, Y.; Xia, S. Enhanced Adsorption of Rhodamine B on Modified Oil-Based Drill Cutting Ash: Characterization, Adsorption Kinetics, and Adsorption Isotherm. *ACS Omega* **2021**, *6*, 17086−17094.

(3) Olvera, R. C.; Silva, S. L.; Robles-Belmont, E.; Lau, E. Z. Review of nanotechnology value chain for water treatment applications in Mexico. *Resour.-Effic. Technol.* **2017**, *3*, 1−11.

(4) Gupta, V. K.; Suhas. Application of low-cost adsorbents for dye removal-a review. *J. Environ. Manage.* **2009**, *90*, 2313−2342.

(5) Zhang, Z.; Gui, W.; Wei, J.; Cui, Y.; Li, P.; Jia, Z.; Kong, P. Functionalized Attapulgite for the Adsorption of Methylene Blue:

Synthesis, Characterization, and Adsorption Mechanism. *ACS Omega* **2021**, *6*, 19586−19595.
(6) Panagopoulos, A. Techno-economic assessment of zero liquid discharge (ZLD) systems for sustainable treatment, minimization, and valorization of seawater brine. *J. Environ. Manage.* **2022**, *306*, 114488.
(7) Panagopoulos, A. Brine management (saline water & wastewater effluents): Sustainable utilization and resource recovery strategy through Minimal and Zero Liquid Discharge (MLD & ZLD) desalination systems. *Chem. Eng. Process.* **2022**, *176*, 108944.
(8) Tian, S.; Xu, S.; Liu, J.; He, C.; Xiong, Y.; Feng, P. Highly efficient removal of both cationic and anionic dyes from wastewater with a water-stable and eco-friendly Fe-MOF via host-guest encapsulation. *J. Cleaner Prod.* **2019**, *239*, 117767.
(9) Kurnia, I.; Karnjanakom, S.; Irkham, I.; Haryono, H.; Situmorang, Y. A.; Indarto, A.; Noviyanti, A. R.; Hartati, Y. W.; Guan, G. Enhanced adsorption capacity of activated carbon over thermal oxidation treatment for methylene blue removal: kinetics, equilibrium, thermodynamic, and reusability studies. *RSC Adv.* **2022**, *13*, 220−227.
(10) Song, Y.; Tan, J.; Wang, G.; Zhou, L. Superior amine-rich gel adsorbent from peach gum polysaccharide for highly efficient removal of anionic dyes. *Carbohydr. Polym.* **2018**, *199*, 178−185.
(11) Ren, X.; Bai, X.; Hu, M.; Liu, D.; Wu, Y.; Zhang, Z. Water footprint assessment of textile enterprise based on ISO14046. *Desalin. Water Treat.* **2019**, *168*, 216−223.
(12) Huang, B.; Zhao, R.; Xu, H.; Deng, J.; Li, W.; Wang, J.; Yang, H.; Zhang, L. Adsorption of Methylene Blue on Bituminous Coal: Adsorption Mechanism and Molecular Simulation. *ACS omega* **2019**, *4*, 14032−14039.
(13) Panagopoulos, A.; Haralambous, K. J. Environmental impacts of desalination and brine treatment-Challenges and mitigation measures. *Mar. Pollut. Bull.* **2020**, *161*, 111773.
(14) Dinh, H. T.; Tran, N. T.; Trinh, D. X. Investigation into the adsorption of methylene blue and methyl orange by UiO-66-NO_2 nanoparticles. *J. Anal. Methods Chem.* **2021**, *2021*, 1.
(15) Niu, H.; Wang, Q.; Liang, H.; Chen, M.; Mao, C.; Song, J.; Zhang, S.; Gao, Y.; Chen, C. Visible-Light Active and Magnetically Recyclable Nanocomposites for the Degradation of Organic Dye. *Materials* **2014**, *7*, 4034−4044.
(16) Zeng, S.; Tan, J.; Xu, X.; Huang, X.; Zhou, L. Facile synthesis of amphiphilic peach gum polysaccharide as a robust host for efficient encapsulation of methylene blue and methyl orange dyes from water. *Int. J. Biol. Macromol.* **2020**, *154*, 974−980.
(17) Zeng, S.; Long, J.; Sun, J.; Wang, G.; Zhou, L. A review on peach gum polysaccharide: Hydrolysis, structure, properties and applications. *Carbohydr. Polym.* **2022**, *279*, 119015.
(18) Singha, I.; Kumar Mishrab, P. Nano-membrane filtration a novel application of nanotechnology for waste water treatment. *Mater. Today: Proc.* **2020**, *29*, 327−332.
(19) Pivokonsky, M.; Kopecka, I.; Cermakova, L.; Fialova, K.; Novotna, K.; Cajthaml, T.; Henderson, R. K.; Pivokonska, L. Current knowledge in the field of algal organic matter adsorption onto activated carbon in drinking water treatment. *Sci. Total Environ.* **2021**, *799*, 149455.
(20) Zhou, L.; Li, N.; Owens, G.; Chen, Z. Simultaneous removal of mixed contaminants, copper and norfloxacin, from aqueous solution by ZIF-8. *Chem. Eng. J.* **2019**, *362*, 628−637.
(21) Nakazawa, Y.; Abe, T.; Matsui, Y.; Shinno, K.; Kobayashi, S.; Shirasaki, N.; Matsushita, T. Differences in removal rates of virgin/decayed microplastics, viruses, activated carbon, and kaolin/montmorillonite clay particles by coagulation, flocculation, sedimentation, and rapid sand filtration during water treatment. *Water Res.* **2021**, *203*, 117550.
(22) Ye, H.; Yang, B.; Wang, Q.; How, Z. T.; Nie, C.; Chelme-Ayala, P.; Guo, S.; Chen, C.; Gamal El-Din, M. Influences of integrated coagulation-ozonation pretreatment on the characteristics of dissolved organic pollutants (DOPs) of heavy oil electric desalting wastewaters. *J. Environ. Manage.* **2021**, *300*, 113756.
(23) Varjani, S.; Rakholiya, P.; Ng, H. Y.; You, S.; Teixeira, J. A. Microbial degradation of dyes: An overview. *Bioresour. Technol.* **2020**, *314*, 123728.
(24) Li, Q.; Li, T.; Wang, Q. Photoelectrocatalytic removal of bisphenol A using [Ru (bpy) 2 (tatp)] 2 modified TiO_2 electrode. *Int. J. Electrochem. Sci.* **2020**, *15*, 6759−6768.
(25) Bacha, A.; Nabi, I.; Cheng, H.; Li, K.; Ajmal, S.; Wang, T.; Zhang, L. Photoelectrocatalytic degradation of endocrine-disruptor bisphenol-A with significantly activated peroxymonosulfate by Co-$BiVO_4$ photoanode. *Chem. Eng. J.* **2020**, *389*, 124482.
(26) Buscio, V.; Crespi, M.; Gutiérrez-Bouzán, C. Sustainable dyeing of denim using indigo dye recovered with polyvinylidene difluoride ultrafiltration membranes. *J. Cleaner Prod.* **2015**, *91*, 201−207.
(27) Paz, A.; Carballo, J.; Pérez, M. J.; Domínguez, J. M. Biological treatment of model dyes and textile wastewaters. *Chemosphere* **2017**, *181*, 168−177.
(28) Zhao, H.; Liang, Z. X.; Gao, Z. Z. Facile preparation of floatable carboxymethyl cellulose-based composite hydrogel for efficient removal of organic dyes. *Colloid Interface Sci. Commun.* **2022**, *49*, 100637.
(29) Setthaya, N.; Pimraksa, K.; Damrongwiriyanupap, N.; Panias, D.; Mekrattanachai, P.; Chindawong, C. Modified zeolite from metakaolin and fly ash as efficient adsorbent for cationic methylene blue dye removal. *Chem. Eng. Commun.* **2022**, 1−17.
(30) Balci, B.; Erkurt, F. E.; Basibuyuk, M.; Budak, F.; Zaimoğlu, Z.; Turan, E. S.; Yılmaz, S. Removal of Reactive Blue 19 from simulated textile wastewater by Powdered Activated Carbon/Maghemite composite. *Sep. Sci. Technol.* **2022**, *57*, 1408−1426.
(31) Bulgariu, L.; Escudero, L. B.; Bello, O. S.; Iqbal, M.; Nisar, J.; Adegoke, K. A.; Alakhras, F.; Kornaros, M. E.; Anastopoulos, I. The utilization of leaf-based adsorbents for dyes removal: A review. *J. Mol. Liq.* **2019**, *276*, 728−747.
(32) Praveen, S.; Jegan, J.; Bhagavathi Pushpa, T.; Gokulan, R.; Bulgariu, L. Biochar for removal of dyes in contaminated water: an overview. *Biochar.* **2022**, *4*, 10.
(33) Soltani, A.; Faramarzi, M.; Mousavi Parsa, S. A. A review on adsorbent parameters for removal of dye products from industrial wastewater. *Water Qual. Res. J.* **2021**, *56*, 181−193.
(34) Kim, I. J.; Zhao, W.; Park, J. G.; Meng, Z. Carbon nanotube filter for heavy metal ion adsorption. *Ceram. Int.* **2021**, *47*, 33280−33285.
(35) Yoshida, S.; Iwamura, S.; Ogino, I.; Mukai, S. R. Adsorption of phenol in flow systems by a monolithic carbon cryogel with a microhoneycomb structure. *Adsorption* **2016**, *22*, 1051−1058.
(36) Qiao, X.; Gao, W.; Liu, X.; Fang, K.; Li, Q.; Lu, X.; Si, J.; Zhang, M.; Liu, D. Preparation of zeolitic imidazolate framework-67/wool fabric and its adsorption capacity for reactive dyes. *J. Environ. Manage.* **2022**, *321*, 115972.
(37) Ma, Y.; Ma, Y.; Zhao, Z.; Hu, X.; Ye, Z.; Yao, J.; Buckley, C. E.; Dong, D. Comparison of fibrous catalysts and monolithic catalysts for catalytic methane partial oxidation. *Renewable Energy* **2019**, *138*, 1010−1017.
(38) Cuo, Z.; Wang, D.; Gong, Y.; Zhao, F.; Liu, H.; Chen, Y. A Novel Porous Ceramic Membrane Supported Monolithic Cu-Doped Mn−Ce Catalysts for Benzene Combustion. *Catalysts.* **2019**, *9*, 652.
(39) Gao, R.; Liu, D.; Huang, Y. P.; Li, G. Preparation of diatomite-modified wood ceramics and the adsorption kinetics of tetracycline. *Ceram. Int.* **2020**, *46*, 19799−19806.
(40) Shigapov, A. N; Graham, G. W; McCabe, R. W; Paputa Peck, M.; Kiel Plummer, H The preparation of high-surface-area cordierite monolith by acid treatment. *Appl. Catal., A* **1999**, *182*, 137−146.
(41) Lv, C.; Chen, H.; Hu, M.; Ai, T.; Fu, H. Nano-oxides washcoat for enhanced catalytic oxidation activity toward the perovskite-based monolithic catalyst. *Environ. Sci. Pollut. Res.* **2021**, *28*, 37142−37157.
(42) Bao, L.; Wu, D. Effect of Acid Treatment on the Catalytic Activity and Mechanical Stability of $SmMnO_3$/Cordierite Monolithic Catalysts. *ChemistrySelect* **2021**, *6*, 7845−7854.
(43) Gatica, J. M.; Harti, S.; Vidal, H. Changing the adsorption capacity of coal-based honeycomb monoliths for pollutant removal

https://doi.org/10.1021/acsomega.3c00305
ACS Omega 2023, 8, 11457−11466

from liquid streams by controlling their porosity. *Appl. Surf. Sci.* **2010**, *256*, 7111−7117.
(44) Hosseini, S.; Moghaddas, H.; Masoudi Soltani, S.; Kheawhom, S. Technological applications of honeycomb monoliths in environmental processes: a review. *Process Saf. Environ. Prot.* **2020**, *133*, 286−300.
(45) Zhang, J.; Yang, H.; Jiang, L.; Dan, Y. Enhanced photo-catalytic activity of the composite of TiO_2 and conjugated derivative of polyvinyl alcohol immobilized on cordierite under visible light irradiation. *J. Energy Chem.* **2016**, *25*, 55−61.
(46) Vicente Rodriguez, M.A.; de D. Lopez Gonzalez, J.; Banares Munoz, M.A. Preparation of microporous solids by acid treatment of a saponite. *Microporous Mater.* **1995**, *4*, 251−264.
(47) Liu, Q.; He, Y. Y.; Yang, J.; Xi, W.; Wen, J.; Zheng, H. M. Modification of Cordierite Honeycomb Ceramics Matrix for DeNOx Catalyst. *MRS Online Proc. Libr.* **2012**, *1449*, 1449.
(48) Yaashikaa, P. R.; Senthil Kumar, P.; Varjani, S.; Saravanan, A. Advances in production and application of biochar from lignocellulosic feedstocks for remediation of environmental pollutants. *Bioresour. Technol.* **2019**, *292*, 122030.
(49) Qiao, X.; Gao, W.; Liu, X.; Fang, K.; Li, Q.; Lu, X.; Si, J.; Zhang, M.; Liu, D. Preparation of zeolitic imidazolate framework-67/wool fabric and its adsorption capacity for reactive dyes. *J. Environ. Manage.* **2022**, *321*, 115972.
(50) Chatterjee, S.; Lee, D. S.; Lee, M. W.; Woo, S. H. Enhanced adsorption of congo red from aqueous solutions by chitosan hydrogel beads impregnated with cetyl trimethyl ammonium bromide. *Bioresour. Technol.* **2009**, *100*, 2803−2809.
(51) Günay, A.; Arslankaya, E.; Tosun, I. Lead removal from aqueous solution by natural and pretreated clinoptilolite: adsorption equilibrium and kinetics. *J. Hazard. Mater.* **2007**, *146*, 362−371.
(52) Cheung, C. W.; Porter, J. F.; McKay, G. Sorption kinetics for the removal of copper and zinc from effluents using bone char. *Sep. Purif. Technol.* **2000**, *19*, 55−64.
(53) Lai, Y.; Wang, F.; Zhang, Y.; Ou, P.; Wu, P.; Fang, Q.; Chen, Z.; Li, S. UiO-66 derived N-doped carbon nanoparticles coated by PANI for simultaneous adsorption and reduction of hexavalent chromium from waste water. *Chem. Eng. J.* **2019**, *378*, 122069.
(54) Gao, M.; Li, B.; Liu, J.; Hu, Y.; Cheng, H. Adsorption behavior and mechanism of p-arsanilic acid on a Fe-based metal−organic framework. *J. Colloid Interface Sci.* **2023**, *629*, 616−627.
(55) Shabaan, O. A.; Jahin, H. S.; Mohamed, G. G. Removal of anionic and cationic dyes from wastewater by adsorption using multiwall carbon nanotubes. *Arabian J. Chem.* **2020**, *13*, 4797−4810.
(56) Liu, J.; Yu, H.; Wang, L. Superior absorption capacity of tremella like ferrocene based metal-organic framework in removal of organic dye from water. *J. Hazard. Mater.* **2020**, *392*, 122274.

https://doi.org/10.1021/acsomega.3c00305
ACS Omega 2023, 8, 11457−11466